

Article pubs.acs.org/JPCA

Competing Segregation of Br⁻ and Cl⁻ to a Surface Coated with a Cationic Surfactant: Direct Measurements of Ion and Solvent Depth **Profiles**

Published as part of The Journal of Physical Chemistry virtual special issue "Emily A. Carter Festschrift".

Xianyuan Zhao,* Gilbert M. Nathanson,* and Gunther G. Andersson*



Cite This: J. Phys. Chem. A 2020, 124, 11102-11110



ACCESS

III Metrics & More

Article Recommendations

attracts more Br than Cl

Supporting Information

ABSTRACT: Ion-surface scattering experiments can be used to measure elemental depth profiles on the angstrom scale in complex liquid mixtures. We employ NICISS (neutral impact collision ion scattering spectroscopy) to measure depth profiles of dissolved ions and solvent in liquid glycerol containing the cationic surfactant tetrahexylammonium bromide (THA+Br-) at 0.013 M and mixtures of NaBr + NaCl at 0.4 M total concentration. The experiments reveal that Br outcompetes Cl in its attraction to surface THA+, and that THA+ segregates more extensively when more Br- ions are present. Intriguingly, the depths spanned by THA+, Br-, and Cl- ions generally increase with Br- bulk concentration, expanding from ~10 to ~25 Å for both Br and Cl depth profiles. This broadening likely occurs because of an increasing pileup of THA+ ions in a multilayer region that spreads the halide ions over a wider depth. The experiments indicate that cationic surfactants enhance Br and Cl concentrations in the surface region far beyond their bulk-phase values, making solutions coated with these surfactants potentially more reactive toward gases that can oxidize the halide ions.

INTRODUCTION

The segregation of halide ions to the surface of water involves the interplay of anion polarizability, size, hydration, and alternation with matching cations over several water layers. 1-8 This anion segregation is greatly magnified when a cationic surfactant such as an alkylammonium ion is added to solution, as revealed by X-ray, 9 neutron, 10 sum frequency generation, 11,12 and photoelectron 13-17 and ion scattering 18-20 experiments and by molecular dynamics simulations. 16,21,22 In this case, local charge attraction drives halide ions to the surface region in numbers that match the surfactant cations, with similar depth profiles that suggest significant lateral intermixing of the anions and cations. This attraction to the surface, for example, underlies the success of foam fractionation in the selective removal of halide anions from solution.²³ Early surface tension measurements revealed that the identity of the anion itself influences the joint segregation of surfactant and halide ions. 24,25 In particular, the extent of tetrabutylammonium (TBA+) cation/halide anion segregation depends systematically on halide identity in the order of $I^- > Br^- > Cl^-$ by ratios of 1.35 > 1.12 > 1 at maximum adsorption.²⁴ Further measurements indicate that the addition of alkali chloride or bromides to longer chain alkylammonium solutions pushes more surfactant cation to the surface, and that, along with the surfactant, added Br ions segregate more than added Cl⁻ ions. ²⁶⁻³⁰ Similar results are obtained for the

preferential enhancement of iodide when NaBr is added to TBAI.³¹

The mutual attraction of halide anion and surfactant cation near the surface provides a powerful means to enhance gasliquid reactions between ambient gases and dissolved Cl-, Br-, and I at ion concentrations well above their bulk-phase concentration. A particularly important reaction in the troposphere is $N_2O_5 + Cl^- \rightarrow ClNO_2 + NO_3^-$, which converts dissolved Cl⁻ in aerosol particles into reactive Cl atoms upon photolysis of gaseous ClNO₂. 32-34 Additionally, the reactions $N_2O_5 + 2Br^-$, $Cl_2 + 2Br^-$, and $O_3 + 2Br^-$ each generate Br_2 , releasing Br atoms upon Br₂ photolysis.^{34–36} The surfactantmediated segregation of halide ions may enhance these reactions in sea spray, which often contain mixtures of water, salt, sugars, and neutral and ionic surfactants.³⁷ Motivated by this possibility, we carried out N2O5 and Cl2 scattering experiments with surfactant-coated glycerol, a solvent which was chosen because of its low vapor pressure ($\sim 10^{-4}$ mbar) and potential for mimicking organic—water mixtures. ^{38–40} Glycerol is a viscous

Received: September 29, 2020 Revised: November 22, 2020 Published: December 16, 2020





(1500 cP at 20 °C), high-permittivity ($\varepsilon = 46$), hydrogenbonded liquid with the structure HOCH₂CH(OH)CH₂OH. Our studies indeed show that the addition of tetrahexylammonium bromide (THA⁺/Br⁻, Figure 1a) to a NaBr/glycerol

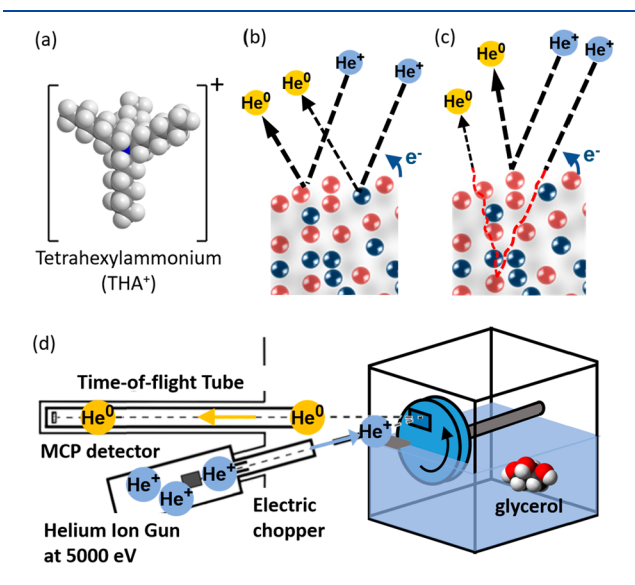


Figure 1. (a) Molecular structure of tetrahexylammonium. Illustration of different energy loss mechanisms: (b) Head-on collisions cause backscattering and large energy transfer, and (c) serial grazing collisions lead to small energy transfers; (d) the NICISS apparatus contains an ion source for 5000 eV He⁺ ions, a rotating wheel reservoir containing glycerol, salt, and surfactant, and a microchannel plate (MCP) for detecting the neutral backscattered He atoms.

solution accelerates reactions of Cl_2 and N_2O_5 with Br^- by ~ 14 -fold over just NaBr alone. In contrast, the addition of the anionic surfactant sodium dodecyl sulfate lowers Cl_2 reactivity by 5-fold, likely due to charge repulsion between Br^- and surface dodecylsulfate anions. We then verified using the ion scattering technique described below that Br^- is strongly drawn to the surface of glycerol by THA^+ and strongly repelled from the

surface by dodecylsulfate.⁴¹ These studies further demonstrate that the Br⁻ enrichment and depletion layers can span dozens of angstroms and are not limited to the outermost monolayer, particularly when NaBr is added to "salt out" THA⁺ to the surface region.

In the current study, we explore ion segregation and solvent depletion in even more complex solutions by adding *both* NaCl and NaBr in different amounts to THABr solutions in glycerol at a constant total ion concentration. The ion scattering probe used here reveals how the additions of both Cl⁻ and Br⁻ control their own spatial distributions and those of THA⁺ and glycerol solvent over the top 70 Å of each solution.

■ EXPERIMENTAL METHODS

Depth Profiles from Ion Scattering. Neutral impact collision ion scattering spectroscopy (NICISS) relies on measurements of the energy loss of high-energy He^+ ions that are neutralized to He atoms upon impact with the solution. 18,42,43 As illustrated in Figure 1b, the neutralized He atoms backscatter from heavier target atoms with more of their initial energy intact. The target mass may then be calculated from the recorded backscattering energy and momentum and energy conservation. This is not the only energy loss, however, as shown in Figure 1c: Most incoming He atoms penetrate into the liquid, undergoing multiple grazing collisions and electronic excitations that transfer small amounts of energy to solutionphase atoms. At some depth, a single head-on collision with a solution-phase atom redirects the He atom backward, which again undergoes numerous small-angle collisions before escaping into the vacuum. These cumulative small energy losses can be calibrated 41,44 and converted into the depth of the solution-phase atom that is struck head-on by the He atom. ⁴⁵ A single time-of-flight (TOF) spectrum thus reveals both the identity of atoms in a thick interfacial region and their depth distributions on the angstrom scale. 46,47

Solution Preparation. THABr, NaBr, and NaCl were purchased from Sigma-Aldrich (purity >99%) and used without further purification. Five THABr/NaBr/NaCl glycerol solutions

Table 1. Bulk and Surface Properties of NaBr/NaCl/THABr/Glycerol Solutions^a

	nominal ratio (Br ⁻ :Cl ⁻)	no added salt b	1:0	1:1	1:5	1:15	1:30
	Br ⁻ mole fraction	1	1	0.5	0.17	0.063	0.032
	Br ⁻ molality/molarity	0.01/0.013	0.31/0.40	0.16/0.206	0.050/0.065	0.020/0.026	0.010/0.013
	Cl ⁻ molality/molarity	0/0	0/0	0.15/0.19	0.26/0.34	0.30/0.39	0.30/0.39
	THA ⁺ molality/molarity	0.01/0.013	0.01/0.013	0.01/0.013	0.01/0.013	0.01/0.013	0.01/0.013
NICISS Measurements of Interfacial Depth Profiles							
	fwhm O depletion (Å)	18	25	24	10	11	10
	fwhm THA+ carbon (Å)	13	25	23	21	19	19
	fwhm Br ⁻ (Å)	11	26	22	13	10	12
	fwhm Cl ⁻ (Å)			26	10	14	13
	(glycerol depletion/4) \times 10 ¹³ molecules cm ⁻²	15	41	39	22	18	18
	THA+ column conc 1013 ions cm-2	13	42	38	25	20	20
	Br ⁻ column conc ^c 10 ¹³ ions cm ⁻²	13	46	26	7.9	3.3	2.2
	Cl ⁻ column conc 10 ¹³ ions cm ⁻²			12	20	29	31
	EF(THA ⁺)	55	165	150	108	84	81
	$EF(Br^{-})$	55	4.6	5.6	5.9	5.7	6.8
	EF(Cl ⁻)			2.1	2.0	2.7	2.9
	selectivity coeff: EF(Br ⁻)/EF(Cl ⁻)			2.7	3.0	2.1	2.3

[&]quot;All column concentrations are integrated over 70 Å. All enhancement factors (EFs) from eq 1 are integrated over 30 Å. "From ref 41. "In comparison, the Br" column concentration for a 0.4 M NaBr solution without THABr is 17×10^{13} ions cm⁻². There is no detectable segregation, such that EF(Br") = 1. See ref 41.

3

were prepared with concentrations listed in Table 1, each containing 0.010 molal (0.013 M) THABr and a total concentration close to 0.3 molal (0.4 M) cations and 0.3 molal anions. Each solution was degassed and dewatered under mild heating and 1 mbar vacuum before use.

Ion-Surface Scattering Apparatus. The scattering machine, depicted in Figure 1d, consists of a He⁺ ion beam generator, liquid scattering target, and neutral He backscattering detector. 41,42 The pulsed 5 keV He⁺ beam was created by electric deflection of the ion beam at 100 kHz with a duty cycle of 0.1% (10 ns pulse width). These He⁺ ions then travel 35.0 cm before striking the liquid. As shown in the figure, a liquid film with a thickness of a few hundred micrometers was created by a rotating stainless-steel disk that was half submerged in solution and continuously scraped by a stainless-steel razor blade. This newly prepared surface was carried by the disk for 3 s before being exposed to the ion beam for 0.1 s. We showed previously that this 3 s delay time is long enough for dissolved THA+ to adsorb to the surface of the scraped solution. 41 The timeaveraged He⁺ flux is 1×10^{11} ions cm⁻² s⁻¹ inside a 1 mm² beam spot on the film, which corresponds to only 0.01% of a monolayer for an 0.3 s exposure time and implies negligible surface destruction. After neutralization and transmission into and out of the liquid, the He atoms were detected over a flight distance L of 135.0 cm by a microchannel plate at a sharp deflection angle of 165°, which was chosen to suppress unwanted signal from multiple medium-angle collisions. 48 Pressures in the scattering chamber were kept below 10^{-5} mbar during the experiments using a liquid nitrogen trap and a 550 L s⁻¹ turbomolecular pump.

■ RESULTS AND DISCUSSION

NICISS experiments were performed using five solutions of NaBr and NaCl mixed with 0.010 molal (0.013 M) THABr in glycerol at 293 K. As listed in Table 1, the Br⁻:Cl⁻ mole ratios were nominally chosen to be 1:0, 1:1, 1:5, 1:15, and 1:30 at a total concentration close to 0.30 molal (0.40 M). In this way, each solution had a halide ion concentration in a 30-fold excess of the THA⁺ concentration.

Qualitative Analysis of Interfacial Composition. Figure 2 displays time-of-flight (TOF) spectra for the $Br^-:Cl^- = 1:0$ and $Br^-:Cl^-=1:30$ solutions. These mixtures are just THABr mixed with a single salt, NaBr (blue) or NaCl (red), respectively. Each spectrum is a plot of the backscattered He signal versus He arrival time at the detector situated 135.0 cm from the liquid sample. The peak with the shortest arrival time near 0 μ s arises from immediate photon emission upon collision of a He⁺ ion with surface atoms. This light pulse is used to determine the zero arrival time for the TOF spectra. Because He atoms backscattering from heavier atoms will lose less energy and thus arrive at the detector over shorter arrival times, the features of the spectra in Figure 2 can be assigned to different elements in solution. The second peak near 3 μ s corresponds to He backscattered from the heaviest atom, Br-, followed by Cl- and then O atoms (from glycerol) and C atoms (from glycerol and THA⁺). Each onset is predicted from the kinematics of isolated He-atom collisions, 41,42 indicating that the edge of each peak or step arises from single collisions with atoms at the outermost surface of the solution. The magnitudes of the signals reflect both the abundance of each atom in the near-interfacial region (up to $\sim 70 \text{ Å}$) and their He scattering cross sections (Br⁻ > Cl⁻ > Na⁺ > O > N > C). Note that Na⁺ and the N atom from THA⁺ are not visible in the spectrum because their interfacial densities

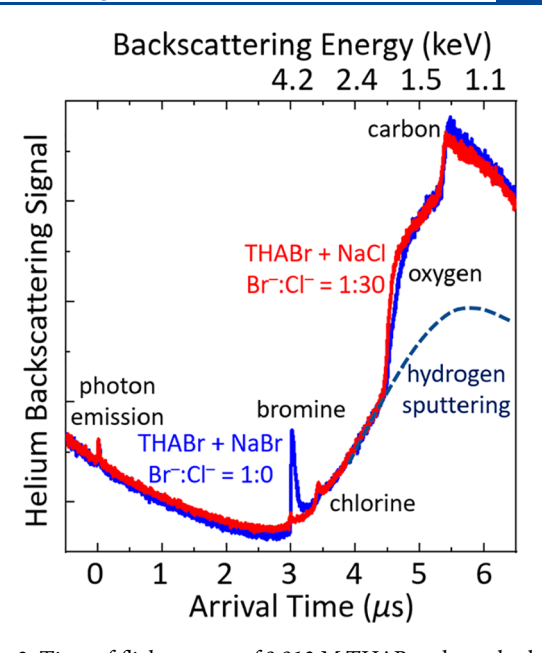


Figure 2. Time-of-flight spectra of 0.013 M THABr—glycerol solutions with added 0.39 M NaCl (red) and added 0.39 M NaBr (blue). The arrival times are calibrated by setting the photon emission to 4.5 ns (the time for a photon to travel from liquid to detector). The dark blue dashed line is a fit to the hydrogen sputtering signal.

are too low to be detected. Each spectrum also contains a large rising background from H atoms belonging to surface molecules that are sputtered by high-energy He atoms. This background is fitted and subtracted before the spectrum is analyzed. ⁴⁹

The sloping downward or upward feature at longer arrival times of the edge of each element in Figure 2 contains essential information about their depth profiles. The slight lag in arrival time arises from grazing He-atom collisions in the liquid (Figure 1c) that cause small, semicontinuous energy losses slowing the He atoms and lengthening their arrival time. It is this depth information encoded in the arrival time delay that we wish to extract for each species in solution. Figure 2 already yields qualitative differences between the THABr + NaBr and THABr + NaCl solutions. First, the lower oxygen signal in the bromideonly spectrum (blue) reveals that the glycerol solvent is more depleted near the surface with added NaBr than with added NaCl. As indicated by the higher carbon signal in the bromideonly solution, this solvent depletion is likely caused by the buildup of extra THA+ ions near the surface. Thus, THA+ segregates more strongly with added Br than with added Cl .. Moreover, the sharp (large) Br and (small) Cl signals at 3.0 and 3.5 μ s tell us that each of these ions segregates to the surface region along with THA⁺. The absence of signal corresponding to Na+ indicates that the cation is not surface-active (in contrast to the distinct Na+ signal from a solution of sodium dodecyl sulfate⁴¹). We proceed below to analyze these spectra quantitatively and extract concentration depth profiles for glycerol, THA+, Br-, and Cl- for each solution.

Deconvolution of Elemental Depth Profiles for Quantitative Analyses. A depth profile is a plot of molar concentration versus depth for a certain species. Because the high kinetic energy He atoms recoil identically from target atoms of different oxidation states, only the nuclear masses of the elements are distinguished by NICISS. The conversion of He arrival times t to He backscattering energy E (where $E = 1/2m_{\rm He}(L/t)^2$) and then to depth z for each element is

described in refs 18, 41, and 44. The key calibration from E to z is determined from measurements of the energy loss of He atoms penetrating through self-assembled monolayers of precisely varying lengths. 41,44 This "stopping power" has been determined to be 4.0 ± 0.7 eV Å⁻¹ at the initial 5 keV He collision energy when He atoms pass through self-assembled alkanethiolate monolayers, whose composition is almost all carbon.⁴⁴ As described in ref 50, the experimental stopping power can also adequately model the energy loss of He atoms passing through organic materials such as THA⁺ and glycerol. The ± 0.7 eV Å⁻¹ uncertainty is equivalent to a uniform compression or expansion of the depth scale up to ~20%. Thus, comparisons of different elemental profiles within a single solution are not affected by this uncertainty in depth. In parallel, the molar concentration (vertical axis) for each depth profile is obtained by scaling the signal at depth z to the signal from 70 Å or deeper in solution, where each element attains its known bulk-phase concentration (see eq 1 of ref 41).

Multiple factors cause the spectrum to broaden and deviate from the actual elemental profiles: the width of the kinetic energy distribution of the incident He⁺ beam, the temporal width of the beam pulse, the distribution of electronic and nuclear energy losses during the head-on backscattering collision, and the broadening of the helium kinetic energy as the He atoms move through the solution (\sim 0.4 eV Å⁻¹). Except for the last one, these broadening factors are measured collectively as the temporal widths (fwhm) of the NICISS spectra following collisions of 5000 eV He⁺ ions with Br, Cl, and O atoms in gas-phase CHBr₃ (39 ns), CHCl₃ (43 ns), and O₂ (83 ns), while the width for carbon (108 ns) is obtained by extrapolation because the gas-phase signal is too low to measure. 41,52

Finally, we use a genetic algorithm to generate a large set of trial profiles that incorporate the factors listed above into the trial set to reproduce the measured spectra. This fitting routine was chosen because it does not assume a predetermined shape for the fitted depth profiles. The distribution of trial profiles is represented by the vertical error bars in the figures. These error bars depict ± 1 standard deviation of the 10 000 trial profiles that are averaged to yield the final profile shown in each graph. Any smooth and area-preserving profile drawn within the error bars may be considered to be a plausible fit to the measured spectrum.

Glycerol Solvent Concentration Depth Profile. Oxygen atoms appear only in glycerol, so they are the signature element of the solvent. The deconvoluted profiles of oxygen are shown in Figure 3 for all five solutions and pure glycerol. In each case, the smooth undulations are not real but arise from the genetic fitting routine. The pure glycerol depth profile starts at 41 M oxygen (3 × 13.7 M glycerol) and drops sharply at zero depth. The absence of a structured rising edge in this profile is in part due to a finite depth resolution estimated to be $\pm 2-3$ Å, which is roughly the size of a glycerol molecule. We note that there is no thermal (capillary wave) broadening of the profile because zero depth starts at the point of the He-surface atom collision regardless of the positions of the neighboring molecules. The He atom also samples a local region in a nearly static configuration: for a penetration depth of 70 Å, the He atom detected in the 165° backscattering geometry emerges 20 Å from the point of collision, traversing 70 Å into solution and 72 Å back out in less than 100 fs.

The most important feature of the O atom profiles in Figure 3 is the diminishing solvent concentration in the surface region

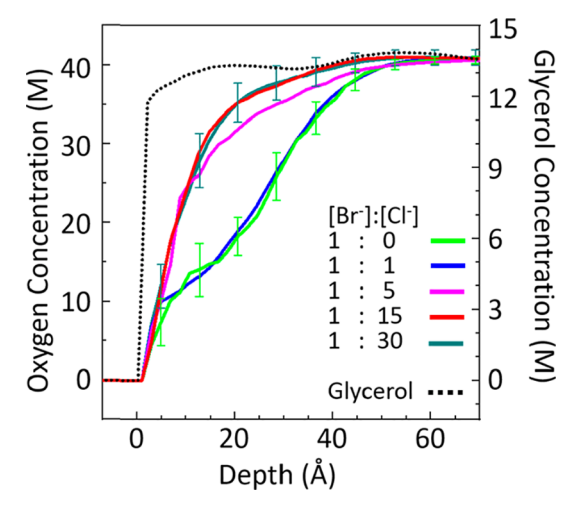


Figure 3. Deconvoluted oxygen profiles of pure glycerol (dashed) and 0.013 M THA⁺ solutions. The labels are the approximate Br⁻:Cl⁻ ratios in solution: 1:0=0.4 M Br⁻/0 M Cl⁻, 1:1=0.21 M Br⁻/0.19 M Cl⁻, 1:5=0.065 M Br⁻/0.34 M Cl⁻, 1:15=0.026 M Br⁻/0.39 M Cl⁻, 1:30=0.013 M Br⁻/0.39 M Cl⁻. Typical error bars are shown for two of the profiles. These error bars represent ± 1 standard deviation of the 10 000 trial profiles generated by the genetic fitting routine.

when the Br $^-$ concentration increases 0.013 M (1:30 curve) to 0.40 M (1:0 curve). We show below that these depletions correlate with the segregation of THA $^+$ to the surface region; the profiles in this sense reveal how the segregated THA $^+$ ions (\sim 10 Å wide) bury glycerol solvent molecules (\sim 5 Å wide). The solvent burial for the 0.40 M NaBr solution extends over 40 Å (8 glycerol layers) and is *not* constrained to a single outermost layer. The substitution of Br $^-$ by Cl $^-$ reduces the amount of displaced glycerol. While the [Br $^-$]:[Cl $^-$] = 1:15 and 1:30 solutions are quite similar in composition and therefore have nearly overlapping glycerol profiles, it is intriguing that the 1:0 and 1:1 glycerol depletions also bunch together. This behavior can be observed directly as well through changes in the THA $^+$ depth profiles shown in the next section.

THA⁺ Carbon Concentration Depth Profiles. To explore how the segregation of THA⁺ ions varies with Br⁻ concentration, we first extract the THA⁺ depth profiles from the carbon signal. This deconvolution proceeds in two steps because carbon atoms are present in both THA⁺ and glycerol (which has equal numbers of C and O atoms). As illustrated in Figure 4a, we first extract the total carbon depth profile and then subtract the oxygen depth profile, which belongs only to glycerol and is assumed to have a profile identical to that of the glycerol carbon. The resulting carbon depth profile can then be assigned to THA⁺ when it is divided by 24 C atoms per molecule.

Figure 4b shows the resulting THA⁺ profiles: THA⁺ increasingly segregates as the Br⁻ mole fraction increases, qualitatively mirroring the depletion of solvent in Figure 3. The peak concentration of ~2.9 M THA⁺ at 10 Å is slightly higher than the 2.3 M concentration of THA⁺/Br⁻ calculated from the molar volume of ~0.43 L/mol for the crystal or when dissolved in organic solvents.^{55,56} In order to quantitatively match THA⁺ adsorption in Figure 4 to glycerol depletion in Figure 3, the volume of the THA⁺ ion must be ~4 times larger than that of a glycerol molecule (as listed in Table 1). This 4:1 ratio is smaller than the 6:1 ratio that is expected on the basis of the 0.43 L/mol volume for THABr and 0.073 L/mol for glycerol. These

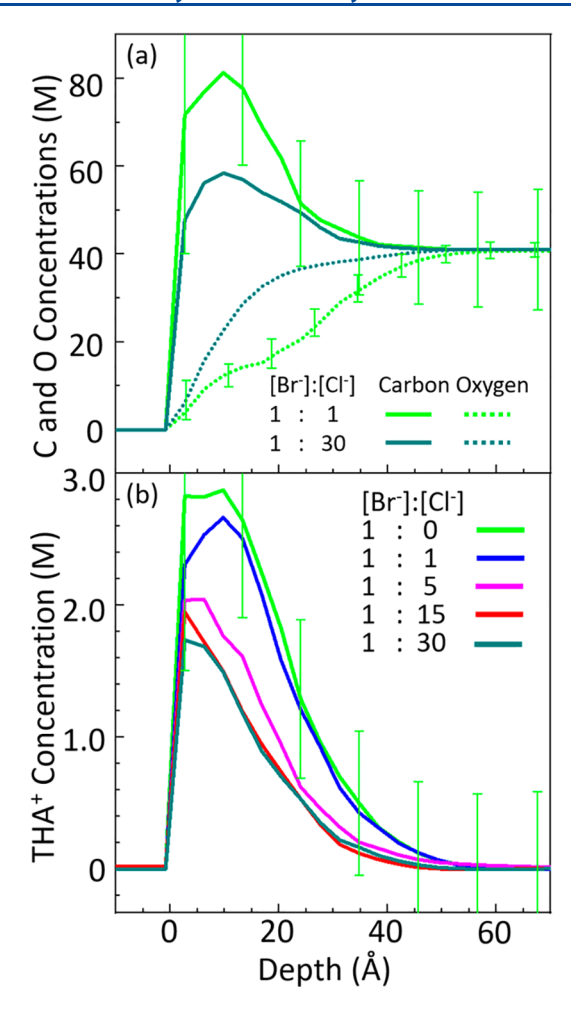


Figure 4. (a) Oxygen depth profiles are subtracted from the total carbon depth profiles (each deconvoluted) to obtain the surfactant carbon profiles for the 1:1 and 1:30 solutions. (b) The resulting THA+ carbon profiles obtained from panel a after dividing by 24 carbon atoms per THA+. The 1:0 to 1:30 labels are the approximate Br-:Cl- ratios in solution.

different ratios may partly arise from some THA⁺ species sticking out at the surface, thereby displacing fewer glycerol molecules, from glycerol molecules intercalating between the hexyl chains, and from errors in assuming identical stopping powers for glycerol and THA⁺. The shapes of the THA⁺ profiles themselves are compared with those of Br⁻ and Cl⁻.

Bromide and Chloride Concentration Depth Profiles. Figure 5 shows the Br profiles in panel a and Cl profiles in panel b from the surface to a depth of 70 Å. As expected, the profiles demonstrate that more Br ions fill the surface region at a higher bulk Br⁻ mole fraction, with an analogous trend for Cl⁻. These concentrations are addressed quantitatively below. We first focus on the widths of the Br and Cl curves in this figure and THA+ widths in Figure 4, which all generally decrease as Clreplaces Br and the THA+ concentration shrinks. As listed in Table 1, the widths (fwhm) range from ~25 Å for Br and THA+ in the THABr + NaBr solution (1:0 curve in Figure 5) to 19 Å for THA+ and 13 Å for Cl- and Br- in the THABr + NaCl solution (1:30 curve). The 25 Å width corresponds to ~2.5 THA⁺ layers, with colocated Br⁻ ions, while the \sim 13 Å width for Cl⁻ and Br⁻ is just over one THA⁺ layer. The larger 19 Å width of THA+ may arise from its finite size, as the ion itself spans roughly 10 Å. The diffuse distribution of the +1 charge over

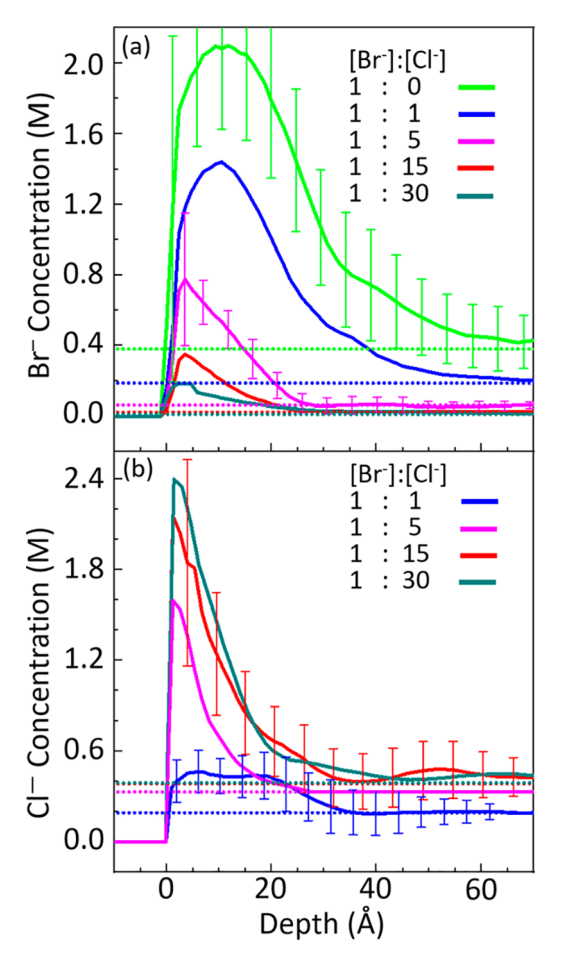


Figure 5. Deconvoluted profiles of the five surfactant solutions. The 1:0 to 1:30 labels are the approximate $Br^-:Cl^-$ ratios in solution. (a) Br^- depth profiles and (b) Cl^- depth profiles. See Table 1 for a numerical analysis of the profiles. The dotted lines indicate the bulk concentrations of Br^- or Cl^- in each solution.

much of the alkyl chains in tetraalkylammonium ions 57 may in turn cause the Br $^-$ and Cl $^-$ ions to distribute broadly over the THA $^+$ layers. Table 1 also shows that the widths of the Cl $^-$ and Br $^-$ profiles roughly match those of the glycerol (O atom) depletion as surfactant and halide ions displace solvent.

One key lesson that emerges from Figures 3, 4, and 5 is the "salting out" or expulsion of THA+ into multiple surface layers as extra Br is substituted for extra Cl, accompanied by the halide ions themselves to maintain local electrical neutrality. The increasingly thick surfactant and halide ion regions emphasize that expulsion is not limited to a single outermost layer when $[Br^-] \ge [Cl^-]$, as shown in Table 1. We hope in future studies to compare the thickness of this region to depth profiles of the same ionic surfactant in water and other solvents. One prior comparison to water is a NICISS study of 0.01 molal tetrabutylammonium iodide (TBA+/I-) in 2.4 molal LiCl in ref 20, which reveals that the iodide profile decays over just a few angstroms, with a falloff that is sharper than for bromide in Figure 5. These different widths may reflect the smaller size of TBA+ than THA+ and of water than glycerol, the weaker surfactant behavior of TBAI than THABr, and the different dielectric constants and structures of the two solvents.

Integrated Column Concentrations of THA⁺, Br⁻, and Cl⁻. This section and the next address the quantitative segregation of ions to a thick interfacial region by integrating

over the depth profiles. The column (integrated) concentrations of THA⁺, Br⁻, and Cl⁻ are computed from Figures 4 and 5 and plotted against Br⁻ bulk mole fraction in Figure 6. All values are

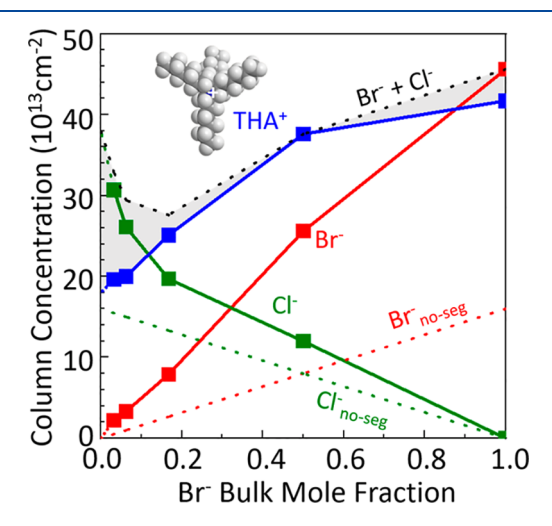


Figure 6. Column concentrations (integrated from 0 to 70 Å) of Br⁻ (red), Cl⁻ (green), and THA⁺ (blue) in units of 10¹³ cm⁻². The red and green dashed curves show the Br⁻ and Cl⁻ column concentrations with no segregation. The black dashed curve is the sum of Br⁻ and Cl⁻ column concentrations, while the gray area is the difference between this curve and the THA⁺ cation concentration, attributable to Na⁺ ions.

also listed in Table 1. They are computed from the concentration depth profile c(z) according to $\int_0^{70} {}^{\rm A}c(z){\rm d}z$, using integration limits from 0 to 70 Å to include all visible interfacial features in each profile. This integral is close to the Gibbs relative adsorption but is more directly interpretable as the absolute adsorption (see Supporting Information). Specifically, Figure 6 shows that THA+ (blue line) segregates more in the presence of Br- than of Cl-. The addition of just NaCl itself, however, is enough to salt out THA+ over the 70 Å region, as the integrated THA+ concentration increases from 13 \times 10¹³ cm⁻² for just 0.013 M THABr ("no added salt" in Table 1) to 20 \times 10¹³ cm⁻² with added 0.4 M NaCl (1:30 solution). It then rises steadily to 42 \times 10¹³ cm⁻² when all of the NaCl is replaced by NaBr (1:0 solution).

Figure 6 further demonstrates that THA⁺ is more effective in attracting Br⁻ than Cl⁻ to the top 70 Å, as expected from previous studies using other techniques. ^{12,24,31} In particular, the column concentration of Br is twice that of Cl when their bulk concentrations are equal (0.5 Br mole fraction). This preferential Br segregation, however, does not stop Cl from dominating the top 70 Å when the bulk Cl⁻ mole fraction rises above ~0.7. Cl replaces Br well enough that the Br column concentration drops below the value of the pure THABr solution at ~0.75 Cl⁻ mole fraction. In all cases, the measured Br and Cl column concentrations (solid lines) are larger than without any segregation (dashed colored lines), for which the actual concentration c(z) is replaced by the bulk concentration $c_{\text{bulk}}(z)$. These no-segregation curves likely correspond to solutions of just NaBr or NaCl in glycerol, as confirmed by our previous study of 0.3 M NaBr, which showed no evidence of Br segregation.43

The sum of the Br⁻ and Cl⁻ column concentrations is represented by the dashed black line in Figure 6. On the basis of electroneutrality maintained over 0–70 Å, the difference between this summed concentration of anions and THA⁺ cation

should be equal to the Na^+ column concentration (highlighted in shade), which is otherwise undetectable by NICISS. The inferred Na^+ column concentration is largest when there is mostly Cl^- in solution. The sharply higher Cl^- column concentration at the left of the figure surprises us, as it seems to infer that both Cl^- and Na^+ are drawn to the surface in the presence of lower (but not zero) interfacial THA^+ concentrations. It will be intriguing in future studies to test this speculation by substituting larger and more polarizable cations such as Cs^+ , which might be independently detectable by NICISS.

Enhancement Factors for THA⁺, **Br**⁻, **and Cl**⁻. In order to quantitatively compare the degree of segregation of THA⁺, Br⁻, and Cl⁻ throughout the surface region, an enhancement factor (EF) can be explicitly computed as the ratio of integrations:

$$EF = \frac{\int_{0}^{z_{\text{cutoff}}} c(z) dz}{\int_{0}^{z_{\text{cutoff}}} c_{\text{bulk}} dz} = \frac{\text{NICISS measured column conc}}{\text{column conc without segregation}}$$

where the numerator is the measured column concentration by NICISS and the denominator is the integration in the absence of any segregation. Both integrals are calculated from 0 Å to a cutoff depth that can be viewed as the boundary of the surface region. Because most profiles have widths of less than 30 Å, as listed in Table 1, the cutoff depth is chosen to be 30 Å (rather than 70 Å) to more cleanly isolate the surface region where interfacial reactions might be thought to occur. Table 1 lists these EF-30 values for THA⁺, Br⁻, and Cl⁻. As expected, the surfactant THA⁺ ion segregates most strongly, as its bulk concentration is only 1/ 30 of the inorganic salt concentration. The THA⁺ enhancements span 84 for the 1:30 solution (nearly all Cl⁻) to 165 for the 1:0 solution (all Br⁻), and in all cases are larger than the EF value of 55 for THABr without any added salt. Thus, both added NaCl and NaBr expel THA+ to the surface region, but Br is roughly twice as effective as Cl⁻.

The segregation of THA⁺ is mirrored in the Br⁻ and Cl⁻ EF-30 values, which are also listed in Table 1. These numbers show that both Br⁻ and Cl⁻ interfacial enhancements increase modestly as NaBr is replaced by NaCl, tracking the THA⁺ enhancement. The ratio of these enhancements, the selectivity coefficient in the last line of Table 1, shows that Br⁻ segregates more than Cl⁻ across the concentration range. The Supporting Information also tabulates EF values at variable, profile-specific cutoff depths corresponding to an 80% drop in peak concentration of each element rather than a uniform 30 Å cutoff for all elements.

Elemental Snapshot of the NaBr:NaCl = 1:5 Mixture. Finally, we compiled all of the measured depth profiles for one solution into a single graph, as shown in Figure 7 for the 1:5 Br-:Cl- solution. This graph reveals that THA+ and its counterions, Cl⁻ and Br⁻, are all greatly enriched within 30 Å from the surface, though with different widths and enhancements. THA+ is itself surface-active and thus rises from a minimal bulk concentration of 0.013 to 2.0 M, a value near that for crystalline THABr packing (2.3 M). Br and Cl are both attracted to the surface by THA+ to balance its charge, but Brsegregates more strongly, as demonstrated by a Br-:Cl- ratio that starts at 1:5 in the bulk and reaches 1:2 over a 30 Å depth. The profiles also suggest that Cl⁻ is slightly more restricted toward the surface than is Br-, with fwhm's of 10 and 13 Å, respectively. This observation, however, must be viewed cautiously because of the high noise level of the chlorine spectra.

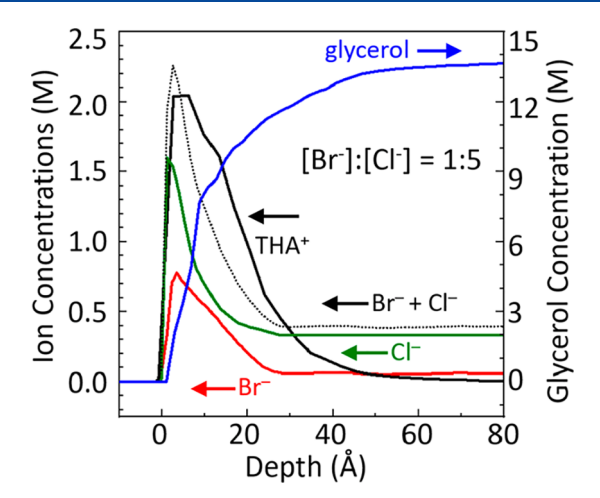


Figure 7. Nearly complete map of species concentration profiles in the 1:5 solution containing 0.013 M THA⁺, 0.065 M Br⁻, and 0.34 M Cl⁻. The sum of Br⁻ and Cl⁻ (dashed) can be compared to the THA⁺ profile. The arrows indicate the vertical axes on which the curves should be read.

Perhaps most importantly, the profiles in Figure 7 reveal that the uppermost 10 Å section is rich in ions that deplete solvent glycerol; they imply a drastic change in composition and structure from a fully solvated environment in the bulk to a solvent-poor, even ionic-liquid-like environment near the surface, where electric charge is not well-screened and the ions must be tightly coordinated. Figures 3, 4, and 5 indicate that this solvent depletion and ion enrichment increase with the Br⁻ mole fraction, becoming even greater for the 1:0 and 1:1 solutions while slightly diminishing for the 1:15 and 1:30 solution. The Supporting Information includes graphs analogous to Figure 7 for all mixtures in order to provide direct comparisons among the species as the Br⁻ and Cl⁻ concentrations are varied.

CONCLUDING REMARKS

The NICISS technique has been applied to a surfactant-mixed salt solution to determine the ways in which both the surfactant cation and competing halide counterions segregate to the surface region. We started with a THABr + NaBr mixture and gradually replaced Br with Cl until the solution composition became THABr + NaCl. As revealed in both the solvent and THA⁺ depth profiles, the adsorbed THA⁺ ions occupy a region that is 2-3 layers thick (26 Å) for THABr + NaBr. Although this cation layer becomes thinner when Cl- dominates the composition, the adsorption layer thickness stops decreasing at 1.5-2 layers (19 Å). This thickness is in contrast to the THABr solution without added salt, whose 13 Å width is closer to a single monolayer. In parallel, the Cl and Br anions respond differently to the segregating THA+ cations. They both act as counterions and are thus both pulled to the surface to balance charge; THA+ makes both halide ions surface-active. However, Br is more effective than Cl in the coupled sense that the THA⁺ column concentration over 70 Å is twice as high with Br as with Cl, and that there are 2-3 times as many interfacial Br as Cl ions with respect to their bulk concentrations. This preferential selectivity for Br may arise from the larger size and higher polarizability of Br^{-,1,3-5,7,8} which reduce the penalty for dragging the ion to the mixed glycerol-charged hydrocarbon surface region.

The findings described above provide insights into the interfacial chemistry of Br⁻ and Cl⁻ in the presence of a cationic

surfactant. In every case, we find that the addition of 0.01-0.03 M THABr to 0.3-0.5 M NaBr-glycerol solutions accelerates Br₂ production by reaction of Cl₂ or N₂O₅ with Br⁻³⁸⁻⁴⁰ This enhanced reactivity is accompanied by a displacement of interfacial glycerol molecules by THA⁺ and Br⁻ ions, implying that the charged hydrophobic environment facilitates halide reactions. 38 However, the addition of NaBr or NaCl in 17- to 30fold ratios to pure THABr-glycerol solutions always decreases Br₂ production, regardless of whether interfacial Br⁻ concentrations increase (for added NaBr) or decrease (for added NaCl). Specifically, Br₂ production by N₂O₅ drops to 75% upon adding 0.5 M NaBr and 37% upon adding 0.5 M NaCl to 0.03 M THABr. 39 We suspect that there are two distinct reasons for these observations. In the case of added NaBr, the interfacial THA+ concentration increases enough for the closely packed alkyl chains to physically block N_2O_5 molecules from reaching neighboring Br $^-$ ions. ^{58–60} Conversely, the dilution of Br $^-$ by Cl⁻ generates a thinner THA⁺ interface but also reduces the Br⁻ concentration, as shown in Table 1. Reactivity thus depends on the interfacial halide concentration and ion environment as well as on gas transport between close-packed surface alkyl chains to bring the gas molecule and halide ion together.

The implications of this work for reactions of oxidizing gases with Br $^-$ and Cl $^-$ in seawater and sea spray come from an extreme extrapolation of our data, as sea-derived mixtures typically have molar Br $^-$:Cl $^-$ ratios of $\sim\!1:650.^{61}$ If our measurements apply as well to aqueous/organic marine environments, they point to selective enhancements of Br $^-$ over Cl $^-$ of only 3-fold or so, as listed in Table 1. Incoming gases will then overwhelming initially encounter Cl $^-$ ions in seawater and sea spray in the absence or presence of cationic surfactants. The conversion of $\rm N_2O_5$ into ClNO $_2$, a neutral molecule that rapidly evaporates, would then be highly favored over BrNO $_2$ or Br $_2$ production even in the presence of cationic surfactants, except in bromide-rich ices found in the Arctic 62 or even in river beds. 63

ASSOCIATED CONTENT

Supporting Information

The Supporting Information is available free of charge at https://pubs.acs.org/doi/10.1021/acs.jpca.0c08859.

Comparison of column concentrations and Gibbs relative adsorptions, depth profile maps analogous to Figure 7 for the 1:0, 1:1, 1:15, and 1:30 Br⁻:Cl⁻ mixtures, and table of enhancement factors (EFs) with profile-specific cutoff depths corresponding to an 80% drop in peak concentration of the depth distribution instead of a constant 30 Å depth (PDF)

AUTHOR INFORMATION

Corresponding Authors

Xianyuan Zhao — Department of Chemistry, University of Wisconsin-Madison, Madison, Wisconsin 53706, United States; ⊚ orcid.org/0000-0001-7926-6562; Email: xzhao287@wisc.edu

Gilbert M. Nathanson — Department of Chemistry, University of Wisconsin-Madison, Madison, Wisconsin 53706, United States; orcid.org/0000-0002-6921-6841; Email: gmnathan@wisc.edu

Gunther G. Andersson – Centre for Nanoscale Science and Technology, Flinders University, Adelaide, South Australia 5001, Australia; o orcid.org/0000-0001-5742-3037; Email: gunther.andersson@flinders.edu.au

Complete contact information is available at: https://pubs.acs.org/10.1021/acs.jpca.0c08859

Notes

The authors declare no competing financial interest.

ACKNOWLEDGMENTS

We are grateful to the National Science Foundation for supporting this research via the Center for Aerosol Impacts on Chemistry of the Environment, a NSF Center for Chemical Innovation (NSF CHE 1801971). The NICISS apparatus was built with a grant from the Australian Research Council (LE160100033). The authors would like to acknowledge the support of the Australian National Fabrication Facility (ANFF) and Australian Microscopy & Microanalysis Research Facility (AMMRF) regarding the use of experimental equipment. The authors further acknowledge Flinders Microscopy and Microanalysis and their expertise. We also thank Christopher Price and Andrew Dunn for their support in machining and electronics design, Liam Howard-Fabretto and Anand Kumar for their assistance with instrumentation, and Ilan Benjamin for discussions of Cl₂ + Br⁻ reactions in the presence of THA⁺.

REFERENCES

- (1) Jungwirth, P.; Tobias, D. J. Specific Ion Effects at the Air/Water Interface. *Chem. Rev.* **2006**, *106*, 1259–1281.
- (2) Ishiyama, T.; Morita, A. Molecular Dynamics Study of Gas-Liquid Aqueous Sodium Halide Interfaces. I. Flexible and Polarizable Molecular Modeling and Interfacial Properties. *J. Phys. Chem. C* **2007**, *111*, 721–737.
- (3) Levin, Y.; dos Santos, A. P.; Diehl, A. Ions at the Air-Water Interface: An End to a Hundred-Year-Old Mystery? *Phys. Rev. Lett.* **2009**, *103*, 257802.
- (4) Otten, D. E.; Shaffer, P. R.; Geissler, P. L.; Saykally, R. J. Elucidating the Mechanism of Selective Ion Adsorption to the Liquid Water Surface. *Proc. Natl. Acad. Sci. U. S. A.* **2012**, *109*, 701–705.
- (5) Stern, A. C.; Baer, M. D.; Mundy, C. J.; Tobias, D. J. Thermodynamics of Iodide Adsorption at the Instantaneous Air-Water Interface. *J. Chem. Phys.* **2013**, *138*, 114709.
- (6) Luo, G. M.; Bu, W.; Mihaylov, M.; Kuzmenko, I.; Schlossman, M. L.; Soderholm, L. X-ray Reflectivity Reveals a Nonmonotonic Ion-Density Profile Perpendicular to the Surface of ErCl₃ Aqueous Solutions. *J. Phys. Chem. C* **2013**, *117*, 19082–19090.
- (7) Perrine, K. A.; Parry, K. M.; Stern, A. C.; Van Spyk, M. H. C.; Makowski, M. J.; Freites, J. A.; Winter, B.; Tobias, D. J.; Hemminger, J. C. Specific Cation Effects at Aqueous Solution-Vapor Interfaces: Surfactant-Like Behavior of Li⁺ Revealed by Experiments and Simulations. *Proc. Natl. Acad. Sci. U. S. A.* **2017**, *114*, 13363–13368.
- (8) Li, J. C.; Wang, F. Surface Penetration without Enrichment: Simulations Show Ion Surface Propensities Consistent with Both Elevated Surface Tension and Surface Sensitive Spectroscopy. *J. Phys. Chem. B* **2019**, *123*, 7197–7203.
- (9) Kashimoto, M.; Shibata, K.; Matsuda, T.; Hoshide, M.; Jimura, Y.; Watanabe, I.; Tanida, H.; Matsubara, H.; Takiue, T.; Aratono, M. Preferential Adsorption of Cationic Surfactant Mixture Studied by Bromide Ion Selective Total-Reflection XAFS Measurement. *Langmuir* **2008**, *24*, 6693–6697.
- (10) Su, T. J.; Lu, J. R.; Thomas, R. K.; Penfold, J. Neutron Reflection from Counterions at the Surface of a Soluble Surfactant Solution. *J. Phys. Chem. B* **1997**, *101*, 937–943.
- (11) Duffy, D. C.; Ward, R. N.; Davies, P. B.; Bain, C. D. Direct Observation of Counterions Bound to a Charged Surfactant Monolayer by Sum-Frequency Vibrational Spectroscopy. *J. Am. Chem. Soc.* **1994**, *116*, 1125–1126.

- (12) Nihonyanagi, S.; Yamaguchi, S.; Tahara, T. Counterion Effect on Interfacial Water at Charged Interfaces and Its Relevance to the Hofmeister Series. J. Am. Chem. Soc. 2014, 136, 6155–6158.
- (13) Bokman, F.; Bohman, O.; Siegbahn, H. O. G. ESCA Studies of Phase-Transfer Catalysts in Solution. 2. Surface Ion-Pairing and Salting-out Effects. *J. Phys. Chem.* **1992**, *96*, 2278–2283.
- (14) Eschen, F.; Heyerhoff, M.; Morgner, H.; Vogt, J. The Concentration Depth Profile at the Surface of a Solution of Tetrabutyammonium Iodide in Formamide, Based on Angle-Resolved Photoelectron Spectroscopy. *J. Phys.: Condens. Matter* **1995**, *7*, 1961–1978
- (15) Watanabe, I.; Takahashi, N.; Tanida, H. Dehydration of Iodide Segregated by Tetraalkylammonium at the Air/Solution Interface Studied by Photoelectron Emission Spectroscopy. *Chem. Phys. Lett.* **1998**, 287, 714–718.
- (16) Winter, B.; Weber, R.; Schmidt, P. M.; Hertel, I. V.; Faubel, M.; Vrbka, L.; Jungwirth, P. Molecular Structure of Surface-Active Salt Solutions: Photoelectron Spectroscopy and Molecular Dynamics Simulations of Aqueous Tetrabutylammonium Iodide. *J. Phys. Chem. B* **2004**, *108*, 14558–14564.
- (17) Wang, C. Y.; Morgner, H. Molar Concentration-Depth Profiles at the Solution Surface of a Cationic Surfactant Reconstructed with Angle Resolved X-Ray Photoelectron Spectroscopy. *Appl. Surf. Sci.* **2011**, 257, 2291–2297.
- (18) Andersson, G.; Morgner, H. Impact Collision Ion Scattering Spectroscopy (ICISS) and Neutral Impact Collision Ion Scattering Spectroscopy (NICISS) at Surfaces of Organic Liquids. *Surf. Sci.* **1998**, 405, 138–151.
- (19) Schulze, K. D.; Morgner, H. Investigation of the Electric Charge Structure and the Dielectric Permittivity at Surfaces of Solutions Containing Ionic Surfactants. *J. Phys.: Condens. Matter* **2006**, *18*, 9823–9839.
- (20) Andersson, G. Energy-Loss Straggling of Helium Projectiles at Low Kinetic Energies. *Phys. Rev. A: At., Mol., Opt. Phys.* **2007**, *75*, 032901.
- (21) Hrobarik, T.; Vrbka, L.; Jungwirth, P. Selected Biologically Relevant Ions at the Air/Water Interface: a Comparative Molecular Dynamics Study. *Biophys. Chem.* **2006**, *124*, 238–242.
- (22) Peng, M.; Nguyen, A. V. Adsorption of Ionic Surfactants at the Air-Water Interface: The Gap between Theory and Experiment. *Adv. Colloid Interface Sci.* **2020**, 275, 102052.
- (23) Grieves, R. B.; The, P. J. W. Anion Exchange Selectivity Coefficients from the Continuous Foam Fractionation of a Quaternary Ammonium Surfactant. *J. Inorg. Nucl. Chem.* **1974**, *36*, 1391–1396.
- (24) Tamaki, K. The Surface Activity of Tetra-n-alkylammonium Halides in Aqueous Solutions. The Effect of Hydrophobic Hydration. *Bull. Chem. Soc. Jpn.* **1974**, *47*, 2764–2767.
- (25) Tanaka, A.; Ikeda, S. Adsorption of Dodecyltrimethylammonium Bromide on Aqueous Surfaces of Sodium Bromide Solutions. *Colloids Surf.* **1991**, *56*, 217–228.
- (26) Okuda, H.; Imae, T.; Ikeda, S. The Adsorption of Cetyltrimethylammonium Bromide on Aqueous Surfaces of Sodium-Bromide Solutions. *Colloids Surf.* **198**7, *27*, 187–200.
- (27) Okuda, H.; Ikeda, S. An Approximate Method for Deriving Surface Excess Densities of Ions on Aqueous Surfaces of Indifferent Ternary Solution. *J. Colloid Interface Sci.* **1991**, *141*, 255–261.
- (28) Para, G.; Jarek, E.; Warszynski, P. The Hofmeister Series Effect in Adsorption of Cationic Surfactants Theoretical Description and Experimental Results. *Adv. Colloid Interface Sci.* **2006**, *122*, 39–55.
- (29) Aratono, M.; Shimamoto, K.; Onohara, A.; Murakami, D.; Tanida, H.; Watanabe, I.; Ozeki, T.; Matsubara, H.; Takiue, T. Adsorption of 1-Decyl-3-methylimidazolium Bromide and Solvation Structure of Bromide at the Air/Water Interface. *Anal. Sci.* **2008**, *24*, 1279–1283.
- (30) Knock, M. M.; Bain, C. D. Effect of Counterion on Monolayers of Hexadecyltrimethylammonium Halides at the Air-Water Interface. *Langmuir* **2000**, *16*, 2857–2865.
- (31) Winter, B.; Weber, R.; Hertel, I. V.; Faubel, M.; Vrbka, L.; Jungwirth, P. Effect of Bromide on the Interfacial Structure of Aqueous

- Tetrabutylammonium Iodide: Photoelectron Spectroscopy and Molecular Dynamics Simulations. Chem. Phys. Lett. 2005, 410, 222-227.
- (32) Bertram, T. H.; Thornton, J. A. Toward a General Parameterization of N_2O_5 Reactivity on Aqueous Particles: The Competing Effects of Particle Liquid Water, Nitrate, and Chloride. *Atmos. Chem. Phys.* **2009**, *9*, 8351–8363.
- (33) Brown, S. S.; Stutz, J. Nighttime Radical Observations and Chemistry. *Chem. Soc. Rev.* **2012**, *41*, 6405–47.
- (34) Abbatt, J. P. D.; Lee, A. K. Y.; Thornton, J. A. Quantifying Trace Gas Uptake to Tropospheric Aerosol: Recent Advances and Remaining Challenges. *Chem. Soc. Rev.* **2012**, *41*, 6555–6581.
- (35) Simpson, W. R.; Brown, S. S.; Saiz-Lopez, A.; Thornton, J. A.; Von Glasow, R. Tropospheric Halogen Chemistry: Sources, Cycling, and Impacts. *Chem. Rev.* **2015**, *115*, 4035–4062.
- (36) Carpenter, L. J.; Nightingale, P. D. Chemistry and Release of Gases from the Surface Ocean. *Chem. Rev.* **2015**, *115*, 4015–4034.
- (37) Cochran, R. E.; Laskina, O.; Trueblood, J. V.; Estillore, A. D.; Morris, H. S.; Jayarathne, T.; Sultana, C. M.; Lee, C.; Lin, P.; Laskin, J.; et al. Molecular Diversity of Sea Spray Aerosol Particles: Impact of Ocean Biology on Particle Composition and Hygroscopicity. *Chem.* **2017**, *2*, 655–667.
- (38) Faust, J. A.; Dempsey, L. P.; Nathanson, G. M. Surfactant-Promoted Reactions of Cl_2 and Br_2 with Br^- in Glycerol. *J. Phys. Chem.* B **2013**, 117, 12602–12612.
- (39) Shaloski, M. A.; Gord, J. R.; Staudt, S.; Quinn, S. L.; Bertram, T. H.; Nathanson, G. M. Reactions of N₂O₅ with Salty and Surfactant-Coated Glycerol: Interfacial Conversion of Br⁻ to Br₂ Mediated by Alkylammonium Cations. *J. Phys. Chem. A* **2017**, *121*, 3708–3719.
- (40) Gord, J. R.; Zhao, X.; Liu, E.; Bertram, T. H.; Nathanson, G. M. Control of Interfacial Cl_2 and N_2O_5 Reactivity by a Zwitterionic Phospholipid in Comparison with Ionic and Uncharged Surfactants. *J. Phys. Chem. A* **2018**, *122*, 6593–6604.
- (41) Zhao, X. Y.; Nathanson, G. M.; Andersson, G. Experimental Depth Profiles of Surfactants, Ions, and Solvent at the Angstrom Scale: Studies of Cationic and Anionic Surfactants and Their Salting Out. *J. Phys. Chem. B* **2020**, *124*, 2218–2229.
- (42) Andersson, G.; Ridings, C. Ion Scattering Studies of Molecular Structure at Liquid Surfaces with Applications in Industrial and Biological Systems. *Chem. Rev.* **2014**, *114*, 8361–8387.
- (43) Andersson, G.; Morgner, H. Thermodynamics and Structure of Liquid Surfaces Investigated Directly with Surface Analytical Tools. *Ann. Phys.* **2017**, *529*, 1600230.
- (44) Andersson, G.; Morgner, H. Determining the Stopping Power of Low Energy Helium in Alkanethiolates with Neutral Impact Collision Ion Scattering Spectroscopy (NICISS). *Nucl. Instrum. Methods Phys. Res., Sect. B* **1999**, *155*, 357–368.
- (45) Andersson, G.; Morgner, H. Investigations on Solutions of Tetrabutylammonium Salts in Formamide with NICISS and ICISS: Concentration Depth Profiles and Composition of the Outermost Layer. Surf. Sci. 2000, 445, 89–99.
- (46) Ridings, C.; Lockett, V.; Andersson, G. Comparing the Charge Distribution along the Surface Normal in the $[C_6 \text{mim}]^+$ Ionic Liquid with Different Anions. *Colloids Surf.*, A **2012**, 413, 149–153.
- (47) Ridings, C.; Andersson, G. Change of Surface Structure upon Foam Film Formation. *ChemPhysChem* **2015**, *16*, 733–738.
- (48) Spitzl, R.; Niehus, H.; Comsa, G. 180-Degrees Low-Energy Impact Collision Ion-Scattering Spectroscopy. *Rev. Sci. Instrum.* **1990**, 61, 760–764.
- (49) Andersson, G.; Krebs, T.; Morgner, H. Activity of Surface Active Substances Determined from Their Surface Excess. *Phys. Chem. Chem. Phys.* **2005**, *7*, 136–142.
- (50) The stopping power used for our glycerol solutions is discussed in note 37 in ref 41, which is paraphrased here. Model calculations referred to in this note predict a 15% increase in stopping power for glycerol versus an all-carbon SAM. No experiments exist yet to corroborate these predictions at 5 keV He collision energy. Experimentally, a recent NICISS study of an oxygen-rich lipid bilayer yielded the same depth as measured by neutron scattering using the all-carbon stopping power, suggesting that it may be used for glycerol and THA⁺ as well. See

- Alharbi, A. R. M.; Andersson, J. M.; Koper, I.; Andersson, G. G. Investigating the Structure of Self-Assembled Monolayers Related to Biological Cell Membranes. *Langmuir* **2019**, *35*, 14213–14221 We therefore use a single stopping power relation for He atoms in all five solutions, deduced from ref 44. This relation is $dE/dz = 0.0445E^{1/2} + 0.845$ where *E* is the He atom kinetic energy and *z* is the depth..
- (51) Andersson, G.; Morgner, H.; Pohl, H. Energy-Loss Straggling of Helium Projectiles at Low Kinetic Energies: Deconvolution of Concentration Depth Profiles of Inorganic Salt Solutes in Aqueous Solutions. *Phys. Rev. A: At., Mol., Opt. Phys.* **2008**, 78, 032904 The last factor is also called "straggling", a process that reflects the statistical nature of the serial grazing collisions along a trajectory. It includes both the angular spread and the energy dispersion in this stochastic process.
- (52) Andersson, G.; Morgner, H.; Schulze, K. D. Surface Properties of Electrolyte Solutions Studied with Ion Beam Analysis. *Nucl. Instrum. Methods Phys. Res., Sect. B* **2002**, *190*, 222–225 This study includes an analogous investigation of the broadening factors at 2.0 keV He⁺ incident energy.
- (53) The THABr ion pair volume is estimated to be ~700 ų from refs 55 and 56, while glycerol is 120 ų from its liquid molarity of 13.7 M. (54) Benjamin, I.; Wilson, M.; Pohorille, A. Scattering of Ne from the Liquid-Vapor Interface of Glycerol A Molecular Dynamics Study. *J. Chem. Phys.* **1994**, *100*, 6500−6507.
- (55) Coker, T. G.; Ambrose, J.; Janz, G. J. Fusion Properties of Some Ionic Quaternary Ammonium Compounds. *J. Am. Chem. Soc.* **1970**, *92*, 5293–5297.
- (56) Zhao, Y.; Liu, H. J.; Min, Z. J.; Wang, J. J. Volumetric and Viscosity Properties for Tetraalkylammonium Bromides and Some Ions in PC Plus THF Mixtures at 298.15 K. *J. Mol. Liq.* **2016**, 223, 1172–1177.
- (57) Heyda, J.; Lund, M.; Ončák, M.; Slavíček, P.; Jungwirth, P. Reversal of Hofmeister Ordering for Pairing of NH₄⁺ vs Alkylated Ammonium Cations with Halide Anions in Water. *J. Phys. Chem. B* **2010**, *114*, 10843–10852.
- (58) Thornton, J. A.; Abbatt, J. P. D. N_2O_5 Reaction on Submicron Sea Salt Aerosol: Kinetics, Products, and the Effect of Surface Active Organics. *J. Phys. Chem. A* **2005**, *109*, 10004–10012.
- (59) McNeill, V. F.; Patterson, J.; Wolfe, G. M.; Thornton, J. A. The Effect of Varying Levels of Surfactant on the Reactive Uptake of N_2O_5 to Aqueous Aerosol. *Atmos. Chem. Phys.* **2006**, *6*, 1635–1644.
- (60) Shaloski, M. A.; Sobyra, T. B.; Nathanson, G. M. DCl Transport through Dodecyl Sulfate Films on Salty Glycerol: Effects of Seawater Ions on Gas Entry. *J. Phys. Chem. A* **2015**, *119*, 12357–12366.
- (61) Bertram, T. H.; Cochran, R. E.; Grassian, V. H.; Stone, E. A. Sea Spray Aerosol Chemical Composition: Elemental and Molecular Mimics for Laboratory Studies of Heterogeneous and Multiphase Reactions. *Chem. Soc. Rev.* **2018**, *47*, 2374–2400.
- (62) Lopez-Hilfiker, F. D.; Constantin, K.; Kercher, J. P.; Thornton, J. A. Temperature Dependent Halogen Activation by N₂O₅ Reactions on Halide-Doped Ice Surfaces. *Atmos. Chem. Phys.* **2012**, *12*, 5237–5247.
- (63) Mitroo, D.; Gill, T. E.; Haas, S.; Pratt, K. A.; Gaston, C. J. CINO₂ Production from N₂O₅ Uptake on Saline Playa Dusts: New Insights into Potential Inland Sources of CINO₂. *Environ. Sci. Technol.* **2019**, 53, 7442–7452.